GANIL

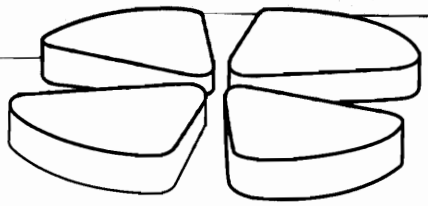

GANIL-P-99-37

PHASE TRANSITION WITH AN ISOSPIN DEPENDENT LATTICE GAS MODEL

Philippe Chomaz[a], Francesca Gulminelli[b] and Véronique Duflot[ab]
[a] *GANIL (DSM-CEA/IN2P3-CNRS), B.P. 5027, F-14076 Caen cédex, France*
[b] *LPC Caen, IN2P3-CNRS, ISMRA et Université , F-14050 Caen cédex, France*
()

Fermilab Library
0 1160 0071565 0

Published in "Isospin Physics in Heavy -Ion Collision at Intermediate Energies" by Bao-An Li and W.Udo Schröder

M.S.

GANIL P 99 37

PHASE TRANSITION WITH AN ISOSPIN DEPENDENT LATTICE GAS MODEL

Philippe Chomaz[a], Francesca Gulminelli[b] and Véronique Duflot[ab]
[a] *GANIL (DSM-CEA/IN2P3-CNRS), B.P. 5027, F-14076 Caen cédex, France*
[b] *LPC Caen, IN2P3-CNRS, ISMRA et Université , F-14050 Caen cédex, France*

()

I. INTRODUCTION

One of the most important challenges of heavy ion physics at intermediate bombarding energies is the identification and characterization of the nuclear liquid-gas phase transition [Si83]. With the increasing availability of quasi complete and exclusive data on the deexcitation of well identified single nuclear sources in heavy ion reactions [Ma97], different indirect evidences of such a transition are rapidly accumulating. On one side, the sudden opening of the multifragmentation [Bi93,Sc96] and vaporization [Ri96] channels can be interpreted as the signature of the boundaries of phase mixture [Gr97,Gu97]. This is reinforced by the fact that at the corresponding excitation energy values the caloric curve [Po95] shows a structure similar to a first order phase transition [Bo98,Gu97]. On the other side, the observation of critical exponents like power laws in the charge distribution of the multifragmenting system [Ha96] can be interpreted as an evidence of the transition.

An important property of nuclear matter is the fact that it is built out of two different fluids: protons and neutrons. This new degree of freedom is important to understand the properties of the equation of state. The first theoretical calculations of the phase transition within finite systems were performed [Ca97,Pa95,Ca98] in the isospin symmetric case. It is well known that in a system with two conserved charges (baryon number and isospin, in the nuclear case) the nature itself of the liquid-gas phase transition is modified: the transition is continuous, phase separation is driven by isovector as well as isoscalar instabilities, the value of critical parameters is modified [Mu95,Ra97]. Since most of the multifragmenting systems produced by heavy ion collisions are far from being isospin symmetric, the comparison of experimental charge distributions with theoretical size distributions can be misleading. Using an exactly solvable model of the liquid-gas phase transition, in this chapter we shall show that if one drops out the mean field approximation, the critical parameters of the phase transition depend only slightly on the asymmetry and this dependence is probably hardly detectable for experimentally available N/Z ratios. However a phenomenon analogous to distillation occurs in the fragmentation of a finite piece of matter containing two fluids. This distillation of neutron matter characterizes the transition. This means that the isospin degree of freedom can be used as a new observable to study the phase transition.

The plan of the chapter is as follows: in the next section the isospin dependent Lattice Gas model will be introduced and its thermodynamics calculated from an exact evaluation of the various entropies and partition sums associated with the different ensembles; section 3 will be devoted to a discussion of the different ways to extract thermodynamical signals, in particular using fluctuations. Our main results on the thermodynamics of the lattice gas model are summarized in section 4. The cluster observables at subcritical and supercritical densities with a special emphasis on finite size distortions of the critical parameters and on the effect of the isospin degree of freedom will be presented in section 5; The distillation of isospin asymmetric systems will be discussed in section 6 and finally section 7 will be devoted to conclusions and outlooks.

Further results obtained within this same model can be found in the contribution of S.Das Gupta to this book.

II. THERMODYNAMICS OF THE LATTICE GAS MODEL

The Lattice Gas Model of Lee and Yang [Ya52] has successfully described the liquid-gas phase transition for atomic systems. This same model has already been applied to nuclear physics for isospin symmetric systems in the gran-canonical ensemble [Ca98,Ca97], with an approximate sampling [Mu97] of the canonical ensemble [Pa95], and for isospin asymmetric systems in the mean field approximation [Ra97,Pa96]. The isospin dependent Lattice Gas Model is isomorphous to a spin 1 Ising model with dipolar and quadrupolar interactions [Si75]. The N sites of a lattice are characterized by an occupation number τ which is defined as $\tau = 0$ for a vacancy, and $\tau = 1(-1)$ for a proton(neutron). Particles occupying nearest neighboring sites interact with an energy ϵ_{τ_i,τ_j}. The Hamiltonian is given by

$$\hat{\mathbf{E}} = \sum_{i=1}^{N} \frac{p_i^2}{2m}|\tau_i| + \frac{1}{2}\sum_{i,j\in\mathcal{N}_i} \epsilon_{\tau_i,\tau_j}\tau_i\tau_j \qquad (1)$$

where the second sum runs only on the neighboring sites $\mathcal{N}_i$ of the site i. The coupling constants ϵ_{τ_i,τ_j} are fixed such as to reproduce the volume and symmetry part of the liquid drop model parametrization, $\epsilon_{1,1} = \epsilon_{-1,-1} \equiv$

$\epsilon_d = 0.$ MeV, $\epsilon_{1,-1} \equiv \epsilon_s = -5.5$ MeV. When no isospin dependence is introduced we use $\epsilon_d = \epsilon_s = -5.5$ MeV. In all the calculations shown below the numerical realization of the model is a three-dimensional cubic lattice of size $S = L^3$.

With the finite range interaction defined above the thermodynamical limit does exist for the infinite system. In this limit all the different statistical ensembles converge to a unique thermodynamics. However, for finite systems the various statistical ensembles are not equivalent because fluctuations cannot be neglected. Therefore, the equations of state will be different from one ensemble to the other. Then we are forced to carefully discuss the various statistical ensembles and their adequacy to the nuclear physics experimental situation.

A. Canonical isochore ensemble

In the liquid-gas phase transition, since the order parameter is the density difference between the two phases, the volume is essential in determining thermodynamical properties. A constant volume ensemble can be trivially generated by considering a fixed constraining cubic box. Many studies have been performed considering periodic boundary conditions in order to avoid the effects of the surface [Ca98]. Systems in a fixed cubic volume have also been investigated [Ca97]. In this section periodic boundary conditions will be systematically applied, while the discussion of surface effects will be postponed to section II E where more realistic spherical systems will be considered.

In the canonical isochore ensemble the system is characterized by a linear size L, a fixed number of particles $A = N + Z$ (or equivalently a density $\rho/\rho_0 = A/L^3$), and a temperature β^{-1}. Statistical averages are taken over events obtained with a standard Metropolis sampling [Me53] of the lattice in the canonical ensemble. In this section, we shall limit our analysis to isospin symmetric systems $N = Z = A/2$.

The canonical thermodynamics of the model is calculated from a direct evaluation of the partition sum Z via an iterative procedure. At a temperature β^{-1}, the occupation probability of an energy state E is

$$P_\beta(E) = \frac{1}{Z_\beta} W(E) e^{-\beta E} \tag{2}$$

where $W(E)$ is the degeneracy of the state. In order to have an exact calculation of the equations of state and of the partition properties of the system we use a standard mass conserving Metropolis method to sample events according to the canonical probability eq.(2). Starting from a lattice configuration characterized by an energy E, the occupations of two randomly selected sites are exchanged leading to a new configuration of energy E' with a probability $exp(-\beta\Delta E)$ with $\Delta E = E' - E$. A large ensemble of preliminary events (typically $2 \cdot 10^7$) is first generated in order to reach statistical equilibrium. Then many configurations (typically $2 \cdot 10^4$) are produced using the same Metropolis algorithm before a single one is stocked to avoid event-to-event correlations and the occupation probability distribution is constructed via

$$P_\beta(E) = \frac{N_\beta(E)}{N_0} \tag{3}$$

Here, N_β is the number of events falling in the energy bin of size ΔE around E, and N_0 is the total number of sampled events. The bin size ΔE is chosen small enough that the results are independent of ΔE.

We have checked that an inversion of eq.(2) leads to an a posteriori estimation of the temperature strictly equal to the input one [Gu99a]. From the comparison of the occupation probabilities at two different temperatures β_1, β_2 one then has

$$Z_1 = Z_2 \frac{N_{\beta_1}(E)}{N_{\beta_2}(E)} e^{-E(\beta_1 - \beta_2)} \tag{4}$$

Since this equation is valid for every energy E it can be used to control the algorithm. Then a best fit of Z_1 can be derived. This can be done iteratively with an initial normalization to the infinite temperature limit where the partition sum is analytical. Once the partition sum is known, all thermodynamical quantities can be computed from the standard statistical definitions in the canonical ensemble.

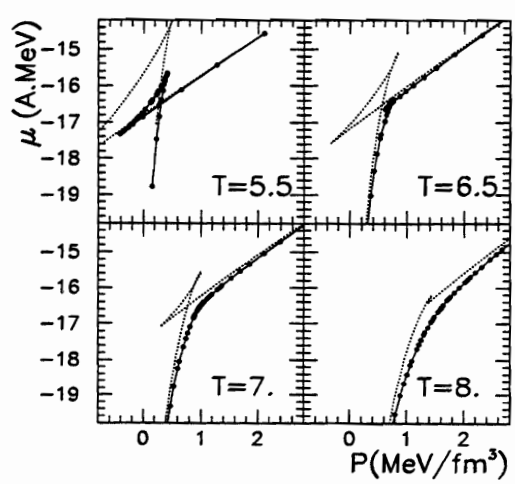

FIG. 1. Chemical potential as a function of pressure at different temperatures for a cubic lattice of size $L = 6$ calculated from the exact partition sum (circles) and with the mean field approximation (dotted line).

As an example, in figure 1 a few isotherms are shown in the chemical potential versus pressure plane for a lattice of size $L = 6$ with a number of particles varying from $A = 10$ to $A = 210$. Even for such small systems, a very clean liquid and gas branch is seen for temperatures up to about 6.5 MeV. Since the crossing point of the two branches represents the coexistence boundary, the coexistence line can be evaluated very precisely from figure 1 leading to a critical temperature $T_c = 6.7$ MeV and a critical exponent $\beta = 0.31$ for the temperature dependence of the order parameter. This value has to be compared with the mean field approximation [Pa95] (shown as dotted line in figure 1) $\beta = 0.5, T_c = 8.1$ and with the expected value in the thermodynamical limit $\beta^{\infty} = 0.33, T_c^{\infty} = 6.16$. It is clear that the finite size of accessible nuclear systems does not imply a drastic deformation of thermodynamical parameters (the corresponding values for $L = 8$ are $T_c = 6.6$ and $\beta = 0.31$). However the speed of convergence towards the thermodynamical limit strongly depends on the observable studied [Ca97].

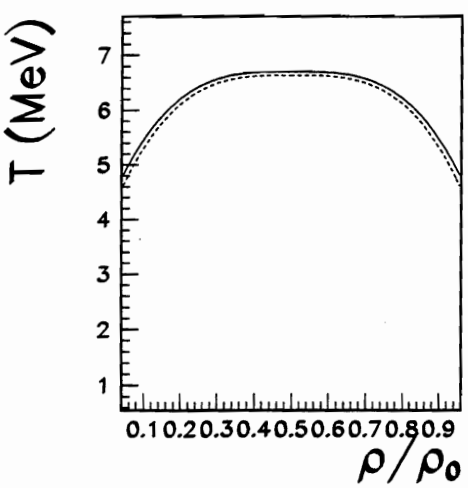

FIG. 2. Coexistence zone computed from the anomaly in the pressure versus chemical potential diagram for a linear size of the lattice L=6 (solid line) and L=8 (dashed line).

B. Microcanonical isochore ensemble

A more fundamental statistical framework for actual applications is the microcanonical ensemble. This ensemble is directly related via its entropy to the elementary density of states. Moreover the microcanonical ensemble is relevant for the analysis of experimental data because of the absence of a heat bath and since using calorimetry techniques the excitation energy can be measured on an event-by-event basis; the events can thus be sorted in constant energy bins, i.e. in microcanonical ensembles. An easy and exact way to access microcanonical quantities is to sort the canonical events according to their total energy. It is important to notice that this procedure may be in some cases numerically time consuming but it is always an exact method to generate constant energy events with the correct microcanonical weight (see eq.(5) below). At a given canonical temperature β^{-1}, the number N_β of events falling in the energy bin E is proportional to the canonical distribution (2), $P_\beta(E)$, and to the total number of events N_0 :

$$\frac{N_\beta(E)}{N_0} = \frac{W(E)}{Z_\beta} \exp(-\beta E) \tag{5}$$

Equation (5) can be inverted in order to extract the density of states $W(E)$ leading to the entropy

$$S(E) \equiv \log(W(E)) \tag{6}$$

This allows a direct estimation of the microcanonical caloric curve

$$T^{-1}(E) \equiv \frac{\partial S(E)}{\partial E} = \beta + \frac{\partial \log N_\beta(E)}{\partial E} \tag{7}$$

which is valid for every β. With a single canonical sampling at an arbitrary β it is in principle possible to directly compute the whole microcanonical caloric curve (7). However for a given β the energies far away from the canonical average $\bar{E}(\beta)$ are hardly sampled in the canonical ensemble. To minimize numerical efforts and statistical errors it is therefore more convenient to perform many canonical samplings at different β associated with average energies scanning the energy region under study.

C. Isobar ensemble: enthalpy properties

In actual nuclear physics experiments, even if different sources with different excitation energies can be prepared, the other thermodynamical parameters can not be independently controlled on an event by event basis even if in some cases they can be measured. In particular the volume is not defined through boundary conditions but is an experimental observable known at best in average. For example the average radius of a selected ensemble of events can be estimated through interferometry or through comparisons with statistical models. From a theoretical point of view one is therefore forced to consider a statistical ensemble for which the volume can fluctuate from event to event. In terms of information theory this implies that at equilibrium the entropy of the system should be maximized under the constraint of a specific value for the average volume. In the absence

of a prefered direction, an average volume can be defined through the one-body observable

$$\hat{\mathbf{V}} = \frac{4\pi}{3} \sum_{i=1}^{N} r_i^3 \tau_i \tag{8}$$

where r_i is the distance to the center of the lattice.

Introducing first a canonical description in which the energy observable $\hat{\mathbf{E}}$ as well as the volume $\hat{\mathbf{V}}$ are known in average we have to introduce the associated Lagrange multipliers β, λ so that the partition function reads

$$Z_{\beta,\lambda} = \sum_{(n)} \exp\left(-\beta E^{(n)} - \lambda V^{(n)}\right) \tag{9}$$

where the sum runs over all possible partitions. Here, $E^{(n)}$ and $V^{(n)}$ are the expectation values of the operators $\hat{\mathbf{E}}$ and $\hat{\mathbf{V}}$ in the nth event, β is the inverse of the canonical temperature, and the quantity $P = -\lambda/\beta$ has the dimension of a pressure. In other words, the experimental fact that the volume is known only in average means that the pressure, interpreted as the Lagrange multiplier associated with the volume observable, can be considered as the relevant state variable. The associated statistical ensemble of events can easily be generated through a canonical sampling using a constrained Hamiltonian $\hat{\mathbf{H}} = \hat{\mathbf{E}} - P\,\hat{\mathbf{V}}$ where $P\,\hat{\mathbf{V}}$ can be considered as a constraining one-body external field. The constrained energy $H = E - PV$ can be interpreted as an enthalpy. The actual value of the pressure parameter must be defined to get the desired average volume.

When the pressure is fixed we can sort the events as a function of the constrained enthalpy H. Then at a given canonical temperature β, the canonical distribution of enthalpies reads

$$P_\beta(H) = \frac{N_\beta(H)}{N_0} = \frac{W(H)}{Z_\beta} \exp(-\beta H) \tag{10}$$

where $N_\beta(H)$ is the number of events falling in the enthalpy bin H out of the total number N_0 of sampled events. Using the general relation $S \equiv \log W$ we can estimate the microcanonical caloric curve via $T^{-1}(H) = \partial_H S(H)$ as in section II B above.

In the calculations shown in this section and in section II D below an isospin symmetric system is considered with a fixed $A = 216$ number of particles. The qualitative results of our analysis are not modified by varying the size of the system; however the actual values of the temperature and heat capacity do depend on A due to finite size effects [Gu99]. For these constrained calculations the size of the lattice is chosen large enough so that the boundary conditions do not affect the numerical sampling. For the results displayed in this section $S = 8000$ is used while in section II D where weaker pressures are considered a lattice size as large as $S = 125000$ is needed. The numerical technique is the same as described in section II A but the lattice occupations are sampled according to the partition function (9).

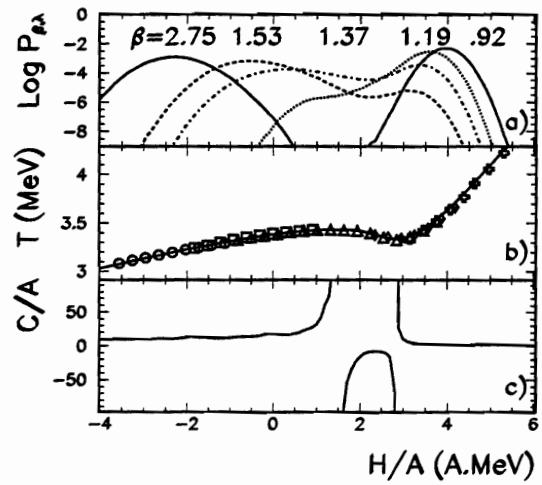

FIG. 3. a) Total constrained enthalpy distributions associated with various canonical β . b) Microcanonical temperature as a function of the enthalpy per particle from various canonical samplings at the different β shown above (symbols) and the corresponding average (line). c) Microcanonical specific heat.

To illustrate a first order phase transition the pressure P is first chosen in such a way that the isobar crosses the canonical coexistence line at about the half of the critical temperature. Figure 3*a* presents the energy distributions at different β. According to equation (10) the logarithm of these probabilities directly gives the entropy apart from a linear correction. Far from the coexistence region the distribution presents the expected Gaussian behavior. When we get close to the coexistence region the observed double bump is a direct evidence of the convex intruder expected in the entropy in the case of a finite microcanonical system undergoing a first order phase transition. This can be better seen on the associated microcanonical caloric curve presented in Figure 3*b*. For each canonical ensemble the total energy exhibits large fluctuations allowing the calculation of the microcanonical temperature over a wide range of energies using equation (7). The fact that the microcanonical temperatures defined from various canonical ensembles at different β all agree within the statistical error bars is a demonstration of the accuracy of the Metropolis sampling. The microcanonical caloric curve presents the expected back-bending in the coexistence region due to the anomalous convexity of the entropy. This induces a negative branch in the microcanonical heat capacity [Th70] $C = (\partial_E T)^{-1}$ as shown in Figure 3*c*. The anomalous curvature of the thermodynamical potential is a clear signature of a first order

phase transition, the distance between the two poles being a direct measure of the latent heat. Increasing the pressure, the two poles get closer up to the critical point where they merge before they disappear.

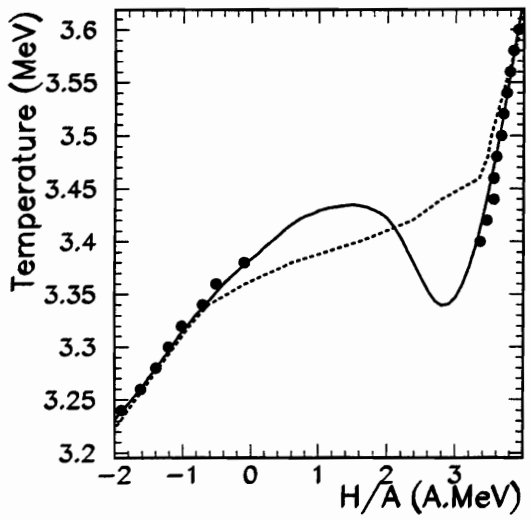

FIG. 4. Microcanonical caloric curve (full line) compared with the most probable (dots) and average (line) canonical enthalpy for each β.

It is interesting to compare the microcanonical and canonical caloric curves as shown in Figure 4. In finite systems two canonical caloric curves can be defined, corresponding to the average and most probable energy associated to a given β. In infinite systems these two energies are equal because fluctuations can be neglected. Far from the phase transition the canonical and microcanonical curves agree. Indeed as seen in Fig. 3a the canonical energy distribution is Gaussian showing that the two ensembles only differ through minor fluctuation corrections. Moreover, from equation (7) we can see that the most probable canonical energy is characterized by the equality of the microcanonical and canonical temperatures. In the coexistence region however the predictions of the two ensembles differ in an noticeable manner. The canonical caloric curves are by definition monovaluated while this restriction does not apply to the microcanonical case: in the back-bending region the canonical caloric curve associated with the most probable energy presents a discontinuity equivalent to the Maxwell construction. The observed energy jump is directly related to the latent heat of the first order phase transition. Because of fluctuations the average energy presents a smoother behavior with however a clear slope change in the transition region. It should be noticed that the partitions which fall in the energy region corresponding to the canonical temperature jump are hardly sampled by the canonical ensemble, but are accessible in the microcanonical ensemble. Therefore, the microcanonical sorting of events allows to study regions of the phase diagram which are forbidden in the canonical formalism. These regions are characterized by specific properties such as negative heat capacities which will be studied in more detail in the next section. In particular it is important to identify experimental observables which can directly inform us about these peculiar properties.

D. Isobar ensemble: volume and energy properties

In the previous section we have concentrated the discussion on the enthalpy properties. However, if the pressure is not fixed, as it is most probably the case in the experimental situation, one should discuss energy and volume independently. The corresponding microcanonical statistical ensemble is defined through the partition function

$$Z_\lambda(E) = \sum_V W_V(E) \exp(-\lambda V) \tag{11}$$

with $W_V(E) = \exp(S(E,V))$ the density of states with an energy E and a volume V . This partition function of the isobar microcanonical ensemble can be computed in an exact way from a standard Metropolis sampling of the corresponding canonical ensemble as in the previous sections.

In the statistical ensemble with fluctuating volume introduced above the energy E and the Lagrange conjugate of the volume λ represent the two state variables of the system. It should be noticed that λ can still be formally related to a pressure via $P = T_\lambda \lambda$. They are associated to two equations of states, giving the microcanonical temperature $T_\lambda^{-1} \equiv \partial_E \log Z_\lambda$ and the average volume $< V >= -\partial_\lambda log Z_\lambda$ as a function of E and λ. The temperature can be evaluated from the energy derivative of the logarithm of the canonical energy distribution $N_{\beta,\lambda}(E)$

$$N_{\beta,\lambda}(E) = \frac{N_0}{Z_\lambda(\beta)} Z_\lambda(E) \exp(-\beta E) \tag{12}$$

where N_0 is the number of states canonically sampled with a given constraining λ, for any thermal Lagrange multiplier β, and the temperature is given by

$$T_\lambda^{-1}(E) \equiv \frac{\partial S_\lambda(E)}{\partial E} = \beta + \frac{\partial \log N_{\beta,\lambda}(E)}{\partial E} \tag{13}$$

Again since this equation is valid for every β, we can use many canonical samplings at different β to derive the same microcanonical caloric curve. The agreement between the different curves provides a strong test of the

numerical sampling [Gu99b]. $< V >$ is calculated by averaging at a given λ over microcanonical events, which are obtained through an energy sorting of canonical partitions.

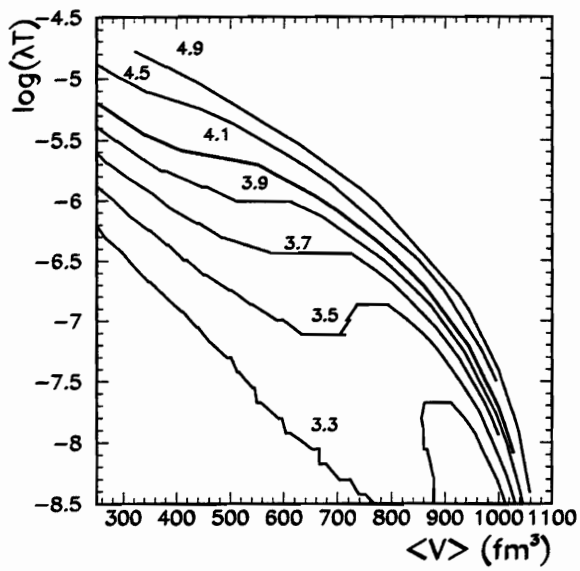

FIG. 5. Correlation between pressure and volume for a system of 216 particles in the microcanonical ensamble with fluctuating volume. The microcanonical temperature is indicated on each isotherm. The thick line gives the critical isotherm.

The $(\lambda T, < V >)$ diagram of the system displayed in Figure 5 shows a striking similarity with the classical (P-V) equation of state of a Van der Waals gas. Far from the coexistence region the curves $P(< V >)$ at constant temperature are monotonous. However, when we get close to the coexistence region we observe an anomalous backbending in the EOS. This induces a negative branch in the compressibility which has already been observed in canonical lattice gas calculations at constant volume [Gu99,Gu99a]. The physical origin of this anomaly is completely different from the backbendings systematically found in the mean field approximation which simply reflect the instability of the homogenous system respect to phase separation. In our exact calculation which naturally includes inhomogeneous partitions conversely this feature corresponds to equilibrium under specific conservation laws (here mass number and energy) [Gu99,Gu99a]. In the microcanonical case the same anomaly is apparent in the equation of state providing the temperature T as a function of the state variables (λ,E) as shown in the two-dimensional caloric curves displayed in figure 6. The backbending of the temperature surface induces a negative branch in the microcanonical heat capacity at constant λ : $C_\lambda^{-1} = \partial T_\lambda(E)/\partial E$.

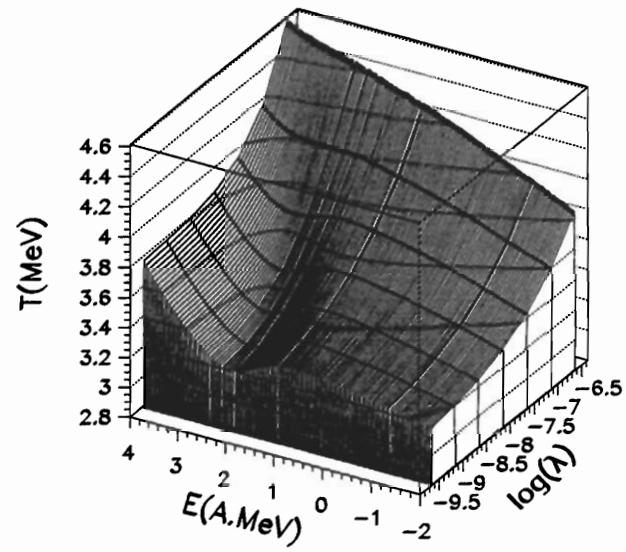

FIG. 6. Temperature as a function of the energy per particle and the Lagrange parameter for a system of 216 particles in the microcanonical ensamble with fluctuating volume.

E. Discussion of the different shapes

The use of the Lagrange multipliers λ in the constrained calculation introduced above leads to a diffuse spherical density distribution shown in figure 7 for two different temperatures and average volumes [Du99]. In order to study the role of the surface conditions, we can compare the constrained calculation with a sharp boundary condition imposed on a spherical surface. The lines in figure 7 represent the respective density profiles for a boundary condition adjusted in such a way that the two calculations lead to identical mean volumes. In the upper part of figure 7 the volume of the sharp sphere is defined to be twice the mass considered so that at high temperature the value of the density corresponds to the critical density $\rho = \rho_c = \rho_0/2$. In the lower part of the figure the volume is doubled to consider a more realistic freeze out condition for nuclear fragmentation. In all figures r_0 represents the elementary mesh size of the lattice. At $T = 3$ MeV the densities are surprisingly close. This demonstrates the preeminence of the interaction on the boundary conditions. Indeed, the fluid forms a drop of liquid which develops a self consistent density profile independently of the surface conditions. At higher temperature the boundary conditions start to be important. At $T = 15$ MeV the system with an imposed sharp boundary finally becomes uniform.

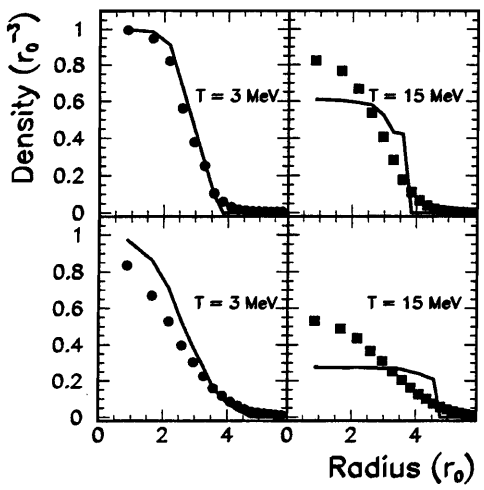

FIG. 7. Density profiles for a system of 108 particles at two temperatures $T = 3$ MeV (left) and $T = 15$ MeV (right). Symbols: Metropolis sampling with a Lagrange pressure such that $< V >= 108$ (upper part) and $< V >= 216$ (lower part). Full lines: sharp boundary conditions in spherical symmetry for the same values of $T, < V >$ as the symbols.

III. PHASE TRANSITION SIGNALS IN THE ISOBAR MICROCANONICAL ENSEMBLE

It has been recently proposed that the microcanonical latent heat can be measured using partial energy fluctuations [Ch99]. The total energy E of the considered system can be decomposed into two independent components, its kinetic and potential energy: $E = E_k + E_p$. In a microcanonical ensemble with a total energy E the total degeneracy factor $W(E) = \exp(S(E))$ is thus simply given by the folding product of the individual degeneracy factors $W_i(E_i) = \exp(S_i(E_i))$ of the two subsystems $i = k, p$. One can then define for the total system as well as for the two subsystems the microcanonical temperatures T_i and the associated heat capacities C_i. Since we are dealing with a classical gas the kinetic equation of state is simply given by $E_k = 3AT_k/2$ and the kinetic heat capacity is a constant, $C_k = 3A/2$. If we now look at the kinetic energy distribution when the total energy is E we get

$$P_k^E(E_k) = \exp(S_k(E_k) + S_p(E - E_k) - S(E)) \quad (14)$$

Using Eq.(14) we directly get that the most probable partitioning of the total energy E between the potential and kinetic components is characterized by a unique microcanonical temperature $\bar{T} \equiv T_k(\bar{E}_k^E) = T_p(E - \bar{E}_k^E)$. Therefore the most probable kinetic energy $\bar{E}_k^E$ can be used as a microcanonical thermometer. Using a Gaussian approximation for $P_k^E(E_k)$ the kinetic energy variance can be calculated as [Le67]

$$\sigma_k^2 = \bar{T}^2 \frac{C_k C_p}{C_k + C_p} \quad (15)$$

where C_k and C_p are the microcanonical heat capacities calculated for the most probable energy partition. Equation (15) can be inverted to extract from the observed fluctuations the heat capacity

$$C \simeq C_k + C_p = \frac{\bar{T}^2 C_k^2}{\bar{T}^2 C_k - \sigma_k^2} \quad (16)$$

When C_p diverges and then becomes negative, σ_k^2 remains positive but overcomes the canonical expectation $\sigma_k^2 = \bar{T}^2 C_k$. This anomalously large kinetic energy fluctuation is a signature of the first order phase transition. This means that kinetic energy fluctuations are an experimentally accessible measure of the heat capacity which indicates divergences and negative branches characteristic of the phase transition.

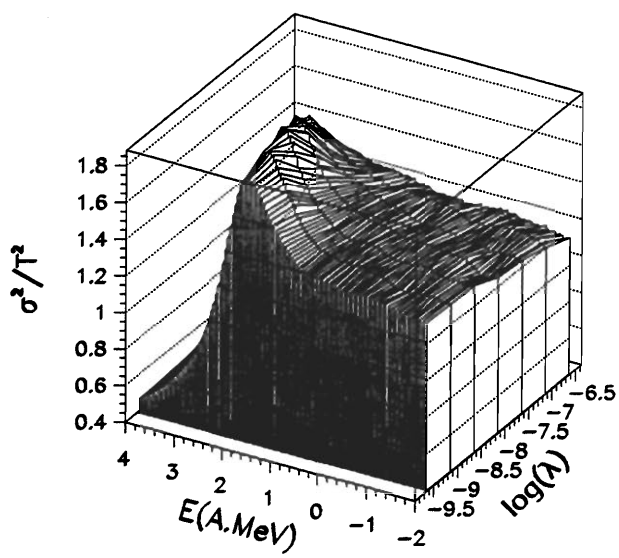

FIG. 8. Normalized kinetic energy fluctuations as a function of the energy per particle and the Lagrange parameter for a system of 216 particles in the microcanonical ensamble with fluctuating volume.

If we now turn back to the fact that the nuclear EOS is two dimensional, two conjugated pairs of thermodynamical variables are needed, one describing the energy part

and the other one the volume. The normalized fluctuations σ_K^2/T^2 obtained in the microcanonical ensemble with a constrained volume are shown in the energy-λ plane in figure 8. From figures 6 and 8 it is apparent that the phase transition signal is visible in the temperature as well as in the fluctuation observable.

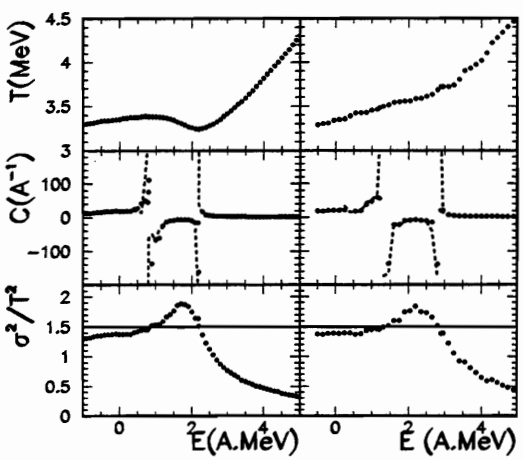

FIG. 9. Thermodynamical quantities in the microcanonical ensemble for a transformation at constant pressure (left part) and at constant volume (right part). Upper panels: caloric curve. Lower panels: normalized kinetic energy fluctuations compared to the canonical expectation (lines). Medium panels: specific heat (symbols) compared to the estimation through eq.(16) (lines).

However the experimentally measured caloric curves are not bidimensional. Indeed, since experimentally the freeze out volume cannot be measured on an event by event basis, fragmentation data can be sorted in excitation energy bins but not in volume bins. This means that experiments are sampling a monodimensional curve on the equation of state surface. The resulting caloric curve therefore depends on the actual transformation i.e. on the actual path followed in the thermodynamical parameters plane. As an example the behavior of the temperature as a function of energy at a constant pressure or a constant average volume in the subcritical region are displayed in the upper part of figure 9. At constant pressure the caloric curves are steeper than the ones at constant λ presented in figure 6 when the system is in the liquid or in the vapor phase; in the coexistence region the isobars are almost identical to the iso-λ's since P and λ differ only by the temperature which is almost constant in the phase transition region, and a backbending is clearly seen. On the other hand at constant volume a smooth behavior is observed with a slope change entering the gas phase, as expected from general thermodynamics (see also [Ca97,Ca99]) . This is due to the fact that the λ parameter varies rapidly in the coexistence region (see fig.5). From these examples one clearly sees that the various transformations leads to very different caloric curves. More generally, it is clear that the backbending of the temperature surface can be avoided depending on the path of the considered transformation and the phase transition signal can be hidden in the observation of the caloric curve.

On the other side partial energy fluctuations are a state variable which does not depend on the transformation from one state to another and can directly give access to the equation of state. From figure 8 we can see that in the whole phase transition region the microcanonical fluctuations present a strong maximum which exceeds the canonical value: an anomalously large fluctuation signal will be always seen if the system undergoes a first order phase transition, independent on the path. As an example the lower part of figure 9 shows a constant p or $< V >$ cut of the bidimensional fluctuation surface shown in figure 8. The quantitative behavior of the specific heat as a function of energy will depend on the specific transformation, but at each point the specific heat extracted from fluctuations will be a direct measure of the underlying equation of state. This is clearly demonstrated in the medium part of figure 8 where the symbols which represent the specific heat C_λ extracted from the equation of state eq.(13) are in very good agreement with the lines which correspond to the fluctuation estimation eq.(15).

IV. CONCLUSIONS ABOUT THERMODYNAMICAL SIGNALS

To summarize the two preceding sections, when finite systems are discussed the statistical ensemble of events is essential to determine the equation of state of the system. In all cases a first order phase transition can be unambigously signed by a convexity anomaly of the relevant thermostatistical potential [Gr95]. This anomaly can be accessed from the study of specific observables depending on the sorting variable which defines the statistical ensemble. In particular, a negative heat capacity is a well defined signal of a first order phase transition only if events are sorted in constant excitation energy bins. In the case of the liquid gas phase transition one is forced to introduce a second thermodynamical variable in order to specify the volume of the system. Then a monodimensional curve such as the measured caloric curves provides insufficient informations to measure the equation of state and can be misleading. On the other hand, kinetic energy fluctuations are independent of the actual trajectory followed in the parameters space and represent a direct measure of the EOS. Considering a statistical ensemble

of states characterized by total energy and an average volume we have shown that abnormal fluctuations are a robust signal of a first order phase transition. In this case kinetic energy fluctuations in the phase transition region are indeed related to the isobar heat capacity C_P which is known to diverge [Ly98].

The connection to experimental fragmentation data is straightforward. The microcanonical ensemble is relevant for the analysis of experimental data because of the absence of a heat bath and since using calorimetry techniques the excitation energy can be measured on an event-by-event basis. As far as the freeze-out volume is concerned, the absence of a constraining box implies that this variable can be known at best in average. Therefore, we expect that the partial energy fluctuations will present a strong anomaly if the multifragmenting nuclear system is undergoing a liquid gas phase transition [Ag99].

V. FINITE SIZE SCALING

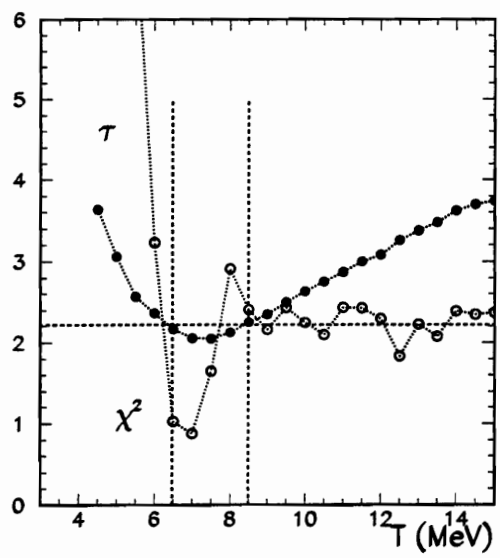

FIG. 10. Slope (filled circles) and corresponding χ^2 (open circles) of the size distribution as a function of temperature for two different system sizes at the critical density. Dashed lines: τ_{max} extracted from the maximum production yields (see text) and corresponding critical temperature interval.

Following the well known example of critical opalescence for macroscopic fluids, we can expect that also in the nuclear case important density fluctuations will characterize the proximity of the critical point leading to a large variety of multifragment configuration patterns. Then the properties of fragment partitions should carry important informations on the presence of a phase transition.

The definition of clusters in the lattice gas combines a site and bond percolation algorithm: two particles are bonded if they

- a) occupy neighbor sites
- b) the kinetic energy of their relative motion $\vec{p}_r^2/2\mu$ does not exceed the binding energy ϵ_{τ_i,τ_j}.

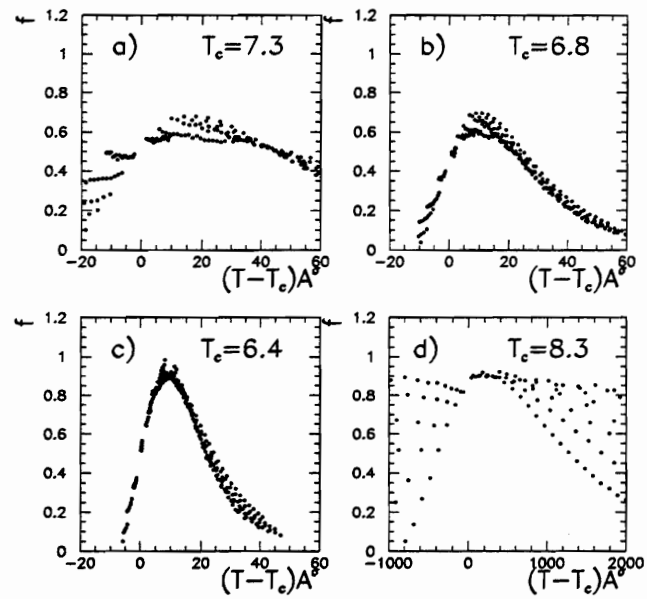

FIG. 11. Scaling function for clusters of size ranging from 4<A<30 and temperature 2<T<20 obtained from eq.(17) with critical exponents extracted with methods 1 (a), 2 (b), and 3 (c,d) described in the text. In figure 3c (d) T_c is given by the lower (upper) bound of the critical temperature region of figure 10.

For details about the definition of clusters we report the reader to refs. [Ca97,Pa95]. Remark that condition *b)* implies that the fragments produced are relatively cold, *i.e.* their thermal excitation energy is lower than the threshold of particle emission; their finite excitation energy is given by their shape rather than by internal degrees of freedom. This definition of clusters guarantees that the thermodynamical critical point exhibits critical fragment size distributions [Co80] and that in the proximity of the critical point the size distribution scales as [St92,Fi67,Ca88]

$$\frac{dN}{dA}(A,T) = A^{-\tau} f\big(A^{\sigma}(T-T_c)\big) \qquad (17)$$

where f is a universal scaling function and τ, σ are critical exponents.

It has already been observed that power laws in the size distribution are not characteristic of the critical point solely, but occur also at supercritical densities along the Kertész line [Ke89,Ca97] and at some subcritical densities at lower temperatures [Pa98a]. In order to better quantify this statement and study the distortions due to finite size effects, we have checked the validity of eq.(17) for different densities and lattice sizes. Different techniques can be proposed to extract the value of the τ exponent. A first possibility [Ha96] (method 1) is to plot the slope of $ln(dN)$ versus $ln(A)$ as a function of temperature; the minimum of this curve (τ_{min}) gives the exponent τ and the corresponding temperature is identified with T_c. Alternatively [Pa95,Pa98a] (method 2) one can use the fact that at $T = T_c$ the χ^2 of the power law fit should be minimum, and the corresponding slope τ_χ of the fit gives the value of τ. Another method (method 3) consists in plotting the maximum production yield $dN_{max}(A)$ of a species of size A as a function of A; one can see from eq.(17) that this quantity should behave as a power law of exponent τ_{max}. Then T_c can be obtained as the temperature at which the power law fit to the size distribution $dN/dA(A)$ gives an exponent $\tau = \tau_{max}$. Note that two solutions may fulfil this requirement.

A. Scaling in the isochore ensemble

These three methods lead to approximately the same value of τ, as it is shown in figure 10; however the corresponding T_c (and consequently the value of σ) are quite different. The values of τ and T_c found systematically lie inside the "critical region" (bounded by the dashed vertical lines of figure 10) obtained with the third method introduced above. This is not a smoothing effect due to the finite size of the system (a well defined critical point of an infinite system being replaced by a wider critical region in the finite one) but it is rather due to the intrinsic imprecision of the methods. As a matter of fact finite size scaling is clearly violated by the use of method 1 (figure 11) implying that this method cannot be used to define the critical point. By requiring that the scaling is verified, the critical temperature can be determined within 0.5 MeV even for a system of a typical nuclear size.

Finite size scaling holds with the same quality at different freeze out densities and lattice sizes. A critical behavior is clearly seen at supercritical densities as well as at subcritical densities. Figure 12 presents the evolution of the critical temperature as a function of the density for a lattice size $L = 8$. This line passes close to the thermodynamical critical point. At high density $\rho \approx 1$ this line reaches the bond percolation critical point. Below the critical point a critical behavior is also seen for a first order phase transition. In this sense there is no contradiction between the scenario of fragmentation at low density inside the coexistence or the spinodal region (first order phase transition) and the observation of critical signals characteristic of a second order phase transition. This property is specific of small systems because it disappears when the volume goes to infinity. Indeed, when the system is very large an infinite fragment is always present in the system for all temperatures up to the coexistence line.

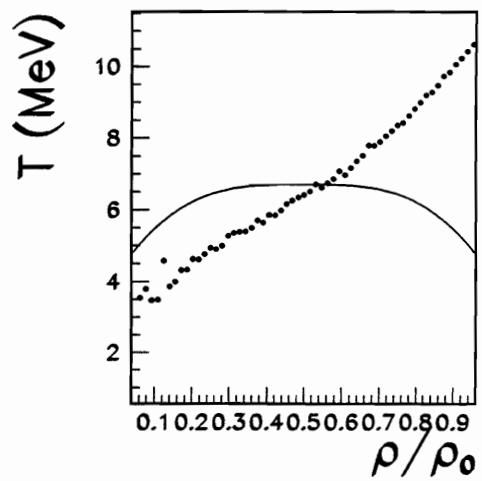

FIG. 12. Full line: coexistence line from thermodynamics (see section 1); symbols: critical curve from fragment size distributions for a cubic lattice of linear dimension $L = 8$.

If the critical temperature is extracted from data by verifying that finite size scaling is respected, critical parameters depend only very slightly on the mass for typical nuclear sources ranging from $A \approx 50$ to $A \approx 300$ and relevant thermodynamical informations can be extracted in spite of finite size effects (figure 13). It should be noticed that at low density in the (experimentally inaccessible) limit of very large systems, scaling becomes very poor. The extracted critical temperature gets close to the coexistence line. This means that in the coexistence region the apparent power laws are not connected to the existence of critical fluctuations of all sizes but rather to the disappearance of the infinite cluster on the coexistence line. Finite size scaling at low densities is therefore a specific property of small systems perfectly compatible with the presence of a first order phase transition. In the thermodynamical limit this scaling is violated as it can be seen by directly looking at the fragment size distribution and as it is shown by the fact that the critical exponents deviate from the expected value of their universality class [Du89] (figure 13a, 13b).

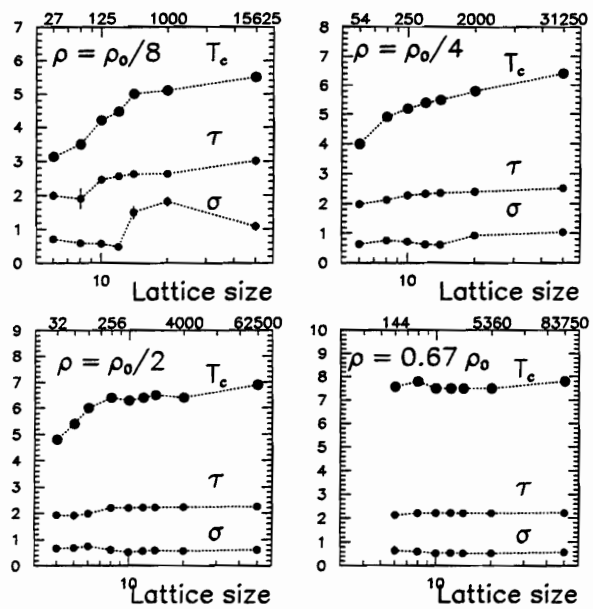

FIG. 13. Critical parameters as a function of the linear size of the lattice (lower scale) or of the mass of the system (upper scale) at different freeze out densities.

B. Role of the volume definition

Besides the role of the finite size, one may wonder about the effects of the surface on the cluster partitions. In order to study the influence of the surface conditions on critical behaviors we have compared the following different systems with the same number of particles :

- a finite cubic system with periodic boundary conditions at half normal density corresponding to the critical density ;
- a finite cubic system without periodic boundary conditions with the same volume as in (1) ;
- a finite sphere with the same volume as in (1) and sharp edges ;
- a finite sphere with a diffuse surface obtained using a constraint on the average volume, the volume being fixed to be the same as the average one of case (3).

The universality of the critical behavior is tested for the diffuse sphere calculation in figure 14. One can see that all the different data points collapse on a single curve demonstrating the validity of the universal scaling. As already observed above, using the requirement that around the critical point fragment production should exhibit a finite size scaling allows to define unambiguously the critical temperature within less than 0.5 MeV even for a finite system of a typical nuclear size.

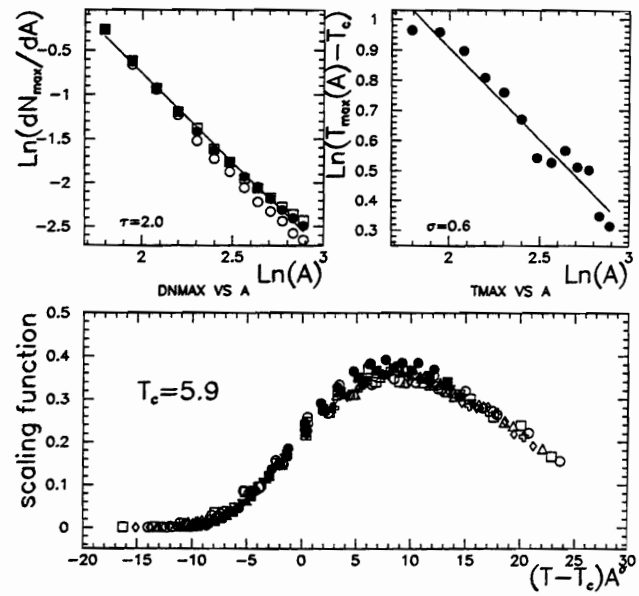

FIG. 14. Scaling function f (see text) extracted from the finite size scaling analysis for a spherical system with $A_0 = 108$ with a diffuse surface for temperatures $3 \leq T \leq 10$ MeV and fragment masses $4 \leq A \leq 20$.

The quality of the critical exponents fit is comparable for all the surface conditions examined and the resulting critical parameters are presented in table 1. The slight variation of the critical temperature can be related to the variations of the density profiles inside the system. If the density of the system is varied between $\rho_0/10$ and ρ_0, the critical exponents remain almost unchanged as well as the agreement between the different surface conditions; only the critical temperature extracted from scaling analysis is seen to decrease monotonically with increasing volume as in the case of periodic boundary conditions (see figure 12).

System	τ	T_c(MeV)	σ
Cubic periodic	2.0 ± 0.1	6.5 ± 0.4	0.8 ± 0.2
Cubic non periodic	2.0 ± 0.1	6.0 ± 0.4	0.7 ± 0.2
Sharp sphere	1.9 ± 0.1	6.2 ± 0.4	0.7 ± 0.2
Diffuse sphere	2.1 ± 0.1	6.1 ± 0.4	0.6 ± 0.2

TABLE I. Critical parameters for the different surface conditions of a system of 108 particles at the critical density

In other words, it is apparent that the change of the surface shape only slightly affects the detailed structure of the scaling function and does not change qualitatively the critical behavior. Power laws in the fragment size distributions are also found in the microcanonical ensemble, at the energy corresponding to the peak of the kinetic energy fluctuations (i.e. at approximately the middle of the negative branch of the heat capacity). Due to the different sorting of events in the microcanonical ensemble however the value of τ is slightly deformed respect to the expected critical exponent of the liquid-gas universality class [Gu99b].

For a realistic application to fragmentation data however other physical ingredients have to be added to the model. In particular the persistence of signals must be verified respect to the long range Coulomb interaction. The fact that minor violations to the scaling in the size of the largest cluster are observed in the macroscopic microcanonical statistical model MMMC [Ja91] which includes the Coulomb field is in this sense very encouraging.

C. Protons and neutrons partitions

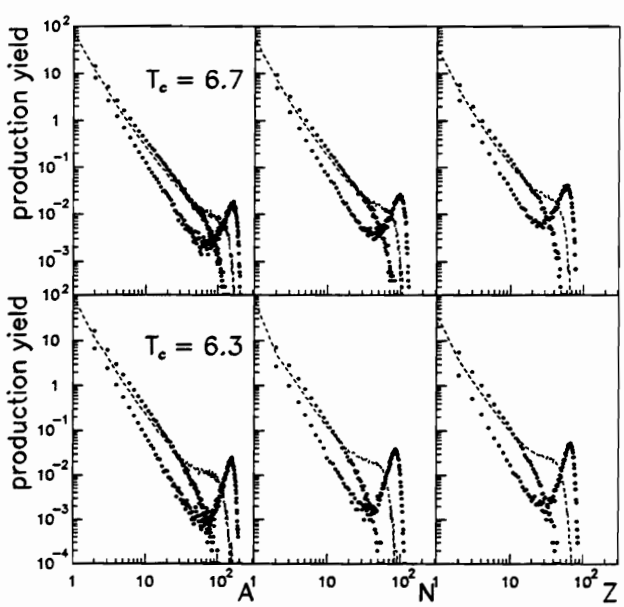

FIG. 15. Fragment mass, neutron number and charge distributions around the critical temperature at half the saturation density for a 8x8x8 cubic lattice with an isospin asymmetry $y = 0$ (upper part) and $y = 0.25$ (lower part).

The results presented in the preceding section have been obtained by assuming an isospin symmetric system, $y = (N - Z)/A = 0$ and considering size distributions. Of course the measurable quantity is the charge rather than the mass distribution. Figure 15 shows that mass, neutron number and proton number distributions exhibit a power law behavior at the same critical temperature. We can also study the proton or neutron distribution for isospin symmetric and asymmetric systems. For an $y \neq 0$ system in the presence of a symmetry energy, *i.e.* a different coupling for isoscalar and isovector pairs, the nature itself of the phase transition is modified [Mu95]. Just to mention a few well known features from macroscopic thermodynamics with two conserved charges, the coexistence curve is transformed into a surface which implies that no discontinuity is observed passing through the phase transition, i.e. as far as transformations are concerned the transition is second order instead of first order; phase separation is triggered by isovector as well as isoscalar instabilities; the isotopic composition of the liquid and gas phase differ. Figure 15 shows that critical behaviors are observed for all the different isotopic composition of the source.

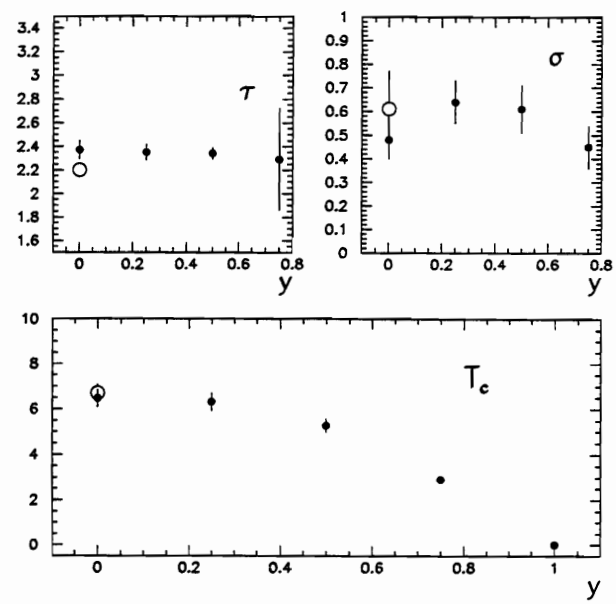

FIG. 16. Critical parameters as a function of the isospin asymmetry of the system for a 8x8x8 cubic lattice at critical density. Open symbols: isospin independent interaction.

The asymmetry dependence of the critical parameters at the critical density is presented in figure 16 for a system of mass $A = 256$. The critical temperature has been obtained with the method 3 of section 4. For comparison, the values obtained in a system of the same size with isospin independent interactions $\epsilon_s = \epsilon_d = -5.5 MeV$ are also given. The same results within error bars are obtained if the parameters are extracted using instead of the total mass of the fragment the total charge or neutron

number.

As expected from universality the critical exponents do not depend on the isospin asymmetry. The observed deviation of τ respect to the isospin independent case is due to the different influence of finite size effects. This can be understood since in an isospin dependent case the fragments lie close to the bottom of the stability valley $N \approx Z \approx A/2$ while in the isospin independent case no restrictions are expected on the partitioning of A nucleons into Z protons and N neutrons. For $A/A_0 \ll 1$ this reduction of the partitions number is an increasing function of A which means that from a combinatorial point of view it is harder to make a big cluster in the isospin dependent system even if the system is isospin symmetric. The difference vanishes as $A \to \infty$ but for the finite system IMF size distributions are naturally steeper, *i.e.* τ is larger than the expected value of the Ising universality class. This result is qualitatively in agreement with the findings of ref. [Pa96].

The critical temperature shows an approximate quadratic dependence on asymmetry (lower part of figure 16) similar to the mean field calculations of refs. [Mu95,Ra97] $T_c(y) - T_c(0) \propto y^\xi$ with $\xi \approx 2$. It should be noticed that since y does not correspond to an order parameter in the considered case the coefficient ξ should not be considered as a critical exponent. Considering the limited variation of y in experiments, even for very exotic nuclei and extremely precise measurements the asymmetry dependence of the critical temperature would be barely visible. On the other hand, the results shown in figure 16 imply that fragmentation data obtained from systems with different asymmetries can be analysed together for a better determination of critical parameters, isospin observables being used to pin down the phase transition and measure thermodynamical quantities.

VI. DISTILLATION OF ISOSPIN ASYMMETRIC SYSTEMS

Isospin can be not only viewed as a degree of freedom but also as an observable: we can hope that next generation detectors for multifragmentation, measuring masses as well as charges of the reaction products, will supply us with a richer two dimensional information reducing the ambiguities of the existing signals for the phase transition. One intriguing possibility is the expectation that for an $y \neq 0$ system inside the coexistence region the vapor phase should be more asymmetric than the liquid phase [Mu95].

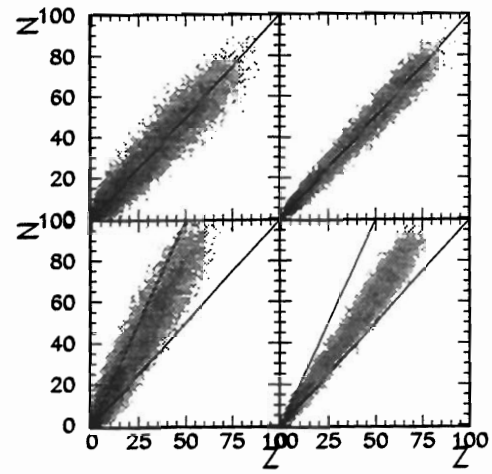

FIG. 17. Distribution of fragments around the critical temperature as a function of their neutron and proton number. Top (bottom) part: $y = 0$ ($y = 0.25$). Left (right) part: $\epsilon_d = \epsilon_s = -5.5$ MeV ($\epsilon_d = 5.5$ MeV, $\epsilon_s = 0$ MeV). Lines: stability $N = Z$ line and isotopic ratio of the initial source.

Figure 17 presents the isobaric distribution of fragments in the proximity of the critical temperature as a function of their neutron and proton number. For an isospin symmetric source the distribution is centered around the $N = Z$ line. When the interaction does not depend on the isospin the observed isobaric distribution is only due to a combinatorial effect. For an isospin dependent interaction the distribution is narrower because the different isobars do not have the same binding energy. In fact the bottom of the stability valley in our simple model which neglects Coulomb effects lies on the $N = Z$ line. Therefore, in addition to the simple combinatorial coefficient the statistical weight due to the variation of the binding energy along an isobaric line leads to a narrowing of the distribution. In the case of an asymmetric source the fragments appear to have the same N/Z ratio as the initial source when the interaction does not distinguish between protons and neutrons. However, when the isospin dependent interaction is switched on we observe that the heavy fragments get closer to the bottom of the stability valley while the light ones present a stronger asymmetry.

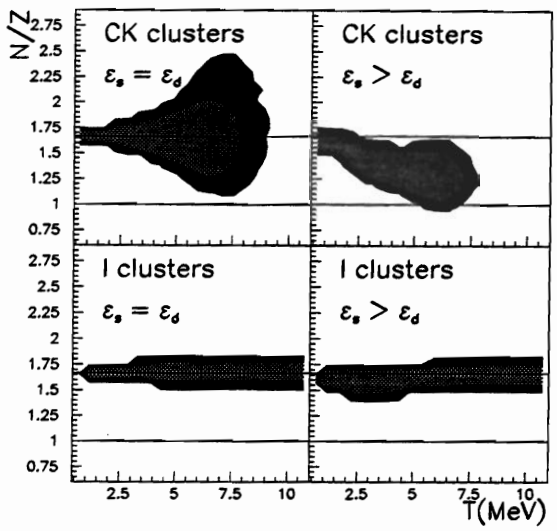

FIG. 18. Ratio between neutron N and proton Z number of produced clusters with $N > 40$ as a function of temperature for a fragmenting system with $N_0 = 160$ and $Z_0 = 96$ at $\rho = \rho_0/2$. Upper (lower) part: Coniglio-Klein (Ising) clusters. Left part: interaction energy $\epsilon_s = \epsilon_d = -5.5$ MeV. Right part: interaction energy $\epsilon_s = -5.5$, $\epsilon_d = 0.$ MeV.

This feature is better visible in figure 18 which displays the isotopic composition of heavy fragments (*i.e.* of the liquid fraction) as a function of temperature for a system with $y = 0.25$. If the interaction energy is assumed independent of isospin, at all temperatures the distribution is centered on the N/Z of the source. This effect is again purely combinatorial and the broadening of the distribution approaching the critical temperature reflects the maximum of fluctuations at the critical point. If symmetry energy is taken into account, the distribution is centered on a value the closer to stability ($N/Z = 1$ in the model, independent on the mass) the higher is the temperature.

The algorithm for cluster definition in the lattice gas model explained in section V guarantees that the excitation energy per nucleon is lower than the threshold of particle emission [Ca97,Pa95], *i.e.* the fragments produced are relatively cold and secondary evaporation is (in average) taken into account. One can then wonder if the observed proton richness (relative to the isotopic composition of the source) of the fragments does not trivially reflect secondary decay. If we construct clusters simply by connecting neighbour occupied sites (Ising clusters), then the average isotopic distribution is given by the lower part of figure 18, which is centered on the combinatorial expectation except at very low temperature. Therefore, even if the cluster proton richness in the model is a genuine signal of phase coexistence one can argue that any model including secondary decay should exhibit the same feature and it may be difficult to disentangle the two effects.

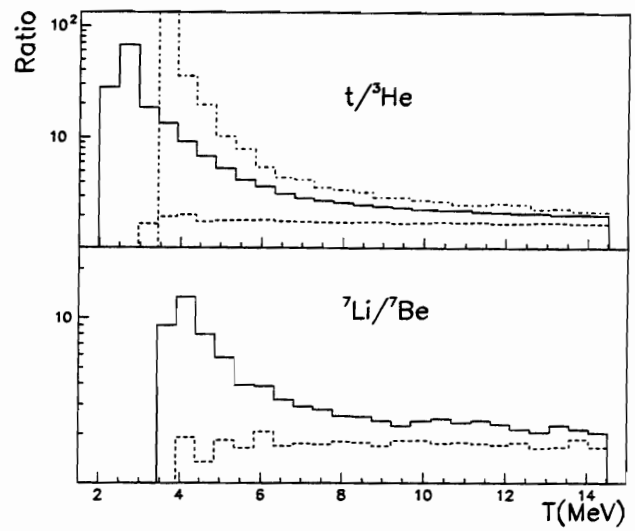

FIG. 19. Relative production yield of light isobars as a function of temperature for a fragmenting system with $N_0 = 160$ and $Z_0 = 96$ at $\rho = \rho_0/2$. Full (dashed-dotted) lines: interaction energy $\epsilon_s = -5.5$, $\epsilon_d = 0.$ MeV; Coniglio-Klein (Ising) clusters. Dashed lines: interaction energy $\epsilon_s = \epsilon_d = -5.5$ MeV; Coniglio-Klein clusters.

A clearer signal of phase coexistence with two conserved charges can be obtained from the analysis of the vapor isotopic composition. Figure 19 shows the ratio between the production yields of different light isobars as a function of temperature with and without isospin dependent interactions. Only at supercritical temperatures the combinatorial value $R = N/Z = 2.1$ is achieved, and the trend is opposite respect to the expected effect of secondary decay. Figure 20 shows the isobaric ratio for different light masses as a function of the asymmetry of the fragmenting system. Above the critical point one can see that this ratio tends toward the isotopic ratio of the source while below the critical point the initial isotopic ratio is strongly enhanced. This very strong enrichment can be related to the existence of two conservation laws, one acting on the proton and the other one on the neutron number. In the presence of a large fragment, i.e. below the critical point, very few protons are free to be captured by the light particles. Indeed, a heavy fragment as close as possible to the bottom of the stability valley is strongly favored from the energetic point of view. Then, as shown by figure 18 above starting with a neutron rich

source we get an almost equilibrated large cluster. Only a few protons are left to be shared between the light fragments leading to the observed strong enhancement of neutron rich "gas"-particles. This is the distillation of neutron matter. It should be noticed that this is a clear signature of the thermodynamical nature of the phase transition.

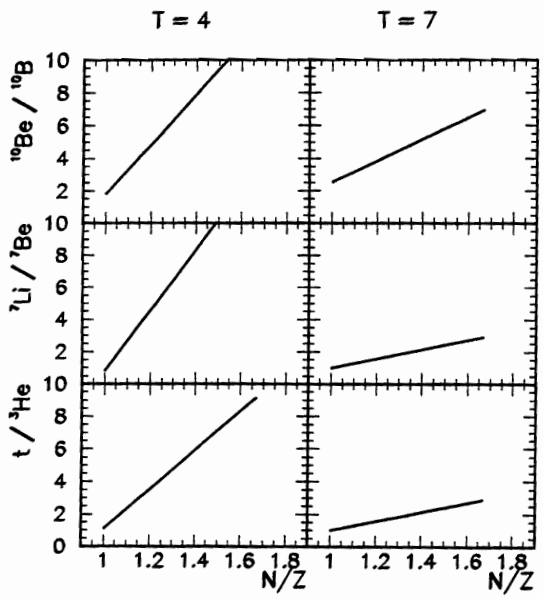

FIG. 20. Relative production yield of light isobars as a function of the N/Z of the fragmenting source and for two different temperatures.

VII. CONCLUSIONS

In this chapter we have looked for relevant signals of the nuclear liquid-gas phase transition within an isospin dependent Lattice Gas model. An exact calculation of the microcanonical and canonical partition function has allowed us to compute the critical point and coexistence line exactly in finite systems. We have also shown that the study of energy partition fluctuations can be a source of information and can provide a measure of the heat capacity. In particular abnormal fluctuation are related to negative heat capacities which are a clear signature of first order phase transition. The critical temperature is also accessible from the fragment production yield, as well as the universal critical exponents of the transition. A full agreement between thermodynamical and fragment variables is obtained if the parameters are extracted from a systematic analysis of size distributions at different temperatures. In this case finite size scaling is remarkably verified over a wide range of sizes and temperatures. The presence at the same time of first and second order transition signals can be understood within a detailed analysis of phase transitions in finite systems. In particular we have demonstrated that a critical behavior in fragment observables can be consistent with the thermodynamics of phase coexistence and the occurrence of a low freeze out density due to finite size effects. Indeed, at variance with the supercritical regime, critical behavior at subcritical densities is a side effect of the finite size of the system which disappears in the infinite limit. However, the dependence with mass being smooth, the observation of critical signals from multifragmenting systems at low densities can provide useful informations on the characteristics and the parameters of the transition. The fact that the critical behavior is not confined to a single thermodynamical point, but can be seen along a whole critical line implies that the temperature and density of the multifragmenting source have to be inferred at the same time from experimental data. Then an interesting observable to better localize the system in the $T-\rho$ plane is given by the isotopic composition of the fragments. We have shown that in the coexistence region the vapor fraction is more asymmetric than the liquid fraction and the signal is not washed out by secondary decay. We have also shown that critical parameters are presenting only a weak dependence on nuclear asymmetry demonstrating that meaningful informations can be extracted from the multifragmentation study of different N/Z sources. Moreover both charge and mass distributions can be used to extract critical behaviors and to sign the distillation phenomenon of asymmetric nuclear matter.

Even if qualitatively the neutron distillation signal has already been experimentally observed [Ye96], for a realistic application to fragmentation data the persistence of signals must be verified respect to the Coulomb interaction.

Ag99 M. D'Agostino et al., nucl-ex/9906004 and to be published in Phys.Lett.B.

Bi93 G. Bizard et al., Phys. Lett. B 302 (1993) 162.

Bo98 J.P.Bondorf, A.S.Botvina, I.N.Mishustin, Phys. Rev. C, submitted.

Ca88 L. Cardy, Current physics - Sources and Comments : vol. 2 : Finite size scaling (North-Holland, Elsevier Science Pub. 1988).

Ca97 X. Campi and H. Krivine, Nucl. Phys. A 620 (1997) 46; J. Pan and S. Das Gupta, Phys.Rev.Lett. 80 (1998)1182.

Ca97 X.Campi and H.Krivine, Nucl. Phys. A 620 (1997) 46 and Physica A, in press.

Ca98 J.M.Carmona, J.Richert, A.Tarancon, Nucl. Phys. A 643 (1998) 115.

Ca99 J.M.Carmona, N.Michel, J.Richert, P.Wagner, nucl-

th/9910061.

Ca98 J.M.Carmona, J.Richert, A.Tarancon, Nucl. Phys. A 643 (1998) 115; F.Gulminelli and P.Chomaz, Phys. Rev. Lett. 82 (1999)1402; Phys. Lett. B 447 (1999) 221.

Ch99 P.Chomaz and F.Gulminelli, Nucl. Phys. A647, 153 (1999).

Co80 A. Coniglio and W. Klein, J. of Phys. A13 (1980) 2775.

Du89 B. Diu et al., Physique Statistique, Hermann (1989) Paris.

Du99 V.Duflot, Ph.Chomaz and F.Gulminelli, preprint GANIL P 99-29 and Phys.Lett.B, in press.

Fi67 M.E. Fisher, Physics vol. 3-5 (1967) 255; M.E. Fisher and M.N. Barber, Phys. Rev. Lett. 28 (1972) 1516.

Gr95 D. H. E. Gross and P.A.Hervieux, Z.Phys. D35 (1995) 27; D.H.E. Gross and E.Votyakov, cond-mat 9911257 .

Gr97 D.H.E. Gross, Phys. Rep. 279(1997) 119.

Gu97 F. Gulminelli and D. Durand, Nucl.Phys. A 615 (1997) 117.

Gu98 F.Gulminelli and Ph.Chomaz, invited paper to the XXXVI Int.Winter Meeting on Nucl.Phys., Bormio, I.Iori ed., (1998) and invited paper to the XIV Winter Wokshop on Nucl.Dynamics, Snowbird, W.Bauer ed., (1998).

Gu99 F.Gulminelli and Ph.Chomaz, Phys. Rev. Lett. 82 (1999) 1402.

Gu99a F.Gulminelli and Ph.Chomaz, Int. Journ. Mod. Phys. E, vol.8,n.6 (1999)1.

Gu99b F.Gulminelli, P.Chomaz and V.Duflot, preprint LPCC 99-17 and to be published in Europhys.Lett.

Ha96 J.A. Hauger et al., Phys.Rev.Lett. 77 (1996) 235; J.B. Elliott et al., Phys. Lett. B 381 (1996) 35; Phys.Lett. B 418 (1998) 34.

Ja91 H.R.Jaqaman and D. H. E. Gross, Nucl.Phys A 524 (1991) 321.

Th70 W. Thirring, Zeit. Phys. 235 (1970) 339.

Ke89 J.Kertész, Physica A 161 (1989) 58.

Ma97 N. Marie et al., Phys.Lett. B 391 (1997) 15, and references therein.

Me53 N. Metropolis et al., J. Chem. Phys. 21 (1953) 1087.

Mu95 H.Mueller and B.D. Serot, Phys.Rev. C 52 (1995) 2072.

Mu97 W.F. Mueller, Phys.Rev. C 56 (1997) 2873.

Ly98 D.Lynden-Bell, Proc. of the XXth IUPAP Int.Conf on Stat. Phys., Paris, July 20-24 (1998) and cond-mat/9812172.

Le67 J.L. Lebowitz et al., Phys. Rev. 153 (1967) 250.

Pa95 J.Pan and S. Das Gupta, Phys.Lett. B 344 (1995) 29; Phys.Rev. C 51 (1995) 1384; Phys.Rev. C 53 (1996) 1319; Nucl.Phys. A 621 (1997) 897.

Pa96 J.Pan and S. Das Gupta, Phys.Rev. C 57 (1998) 1839.

Pa98a J.Pan and S. Das Gupta, Phys.Rev.Lett. 80 (1998)1182.

Po95 J. Pochodzalla et al., Phys.Rev.Lett. 75 (1995) 1040; Y. G. Ma et al, Phys.Lett. B 390 (1997) 41; M.D'Agostino et al., Nucl. Phys. A650 (1999) 329.

Ra97 S.Ray, J.Shamanna, T.T.S. Kuo, Phys.Lett. B 392 (1997) 7.

Ri96 M. F. Rivet et al., Phys. Lett. B 388 (1996) 219; B. Borderie et al.,Phys. Lett. B 388 (1996) 224; Eur. Phys. Jour. A6 (1999) 197.

Sc96 A. Schuttauf et al., Nucl.Phys. A 607 (1996) 457.

Si75 J.Sivardière and J.Lajzerowicz, Phys.Rev. A 11 (1975) 2090.

Si83 P.J. Siemens, Nature 305 (1983) 410; M.W. Curtin et al., Phys. Lett. B 123 (1983) 289.

St92 D.Stauffer and A.Aharony, Introduction to percolation theory (Taylor and Francis, London 1992).

Ya52 C.N. Yang and T.D. Lee, Phys.Rev. 87 (1952) 410.

Ye96 S.J.Yennello et al., Phys. Lett. B 321 (1994) 15; Phys. Lett. B 371 (1996) 186.